Nondestructive analysis of Bennu samples toward comparative studies with Ryugu samples

Ryota FUKAI [1]*, Masahiro NISHIMURA[1], Koki YUMOTO[1], Yuichiro CHO[2], Yuta SHIMIZU[2], Moe MATSUOKA [3], Eri TATSUMI[1], Soichiro FURUKAWA[2], Ryosuke SAKURAI[1], Toru YADA[1], Kentaro HATAKEDA[4], Kasumi YOGATA[1], Yuma ENOKIDO[1], Rui TAHARA [1], Akiko MIYAZAKI[1], Seiya KAWASAKI[1], Rei KANEMARU [1], Seiji SUGITA [2], Shoki MORI[2], Shumpei NAKAHARA[2], Yuta AIKYO [2], Hideaki MIYAMOTO [2], Cedric PILORGET[5,6], Damien LOIZEAU[5], Laura NARDELLI[5], Rachel SHEPPARD[5,7], Cateline LANTZ[5], Lucie RIU[5], Jean-Pierre BIBRING[5], Rosario BRUNETTO[5], Tatsuaki OKADA[1,2], Masanao ABE[1], and Tomohiro USUI[1,2]

[1]Japan Aerospace Exploration Agency, Sagamihara, Japan
[2]The University of Tokyo, Tokyo, Japan
[3]National Institute of Advanced Industrial Science and Technology, Tsukuba, Japan
[4]Marine Works Japan, Yokosuka, Japan
[5]European Space Agency, Madrid, Spain
[6]Institut Universitaire de France, Paris, France
[7]Planetary Science Institute, Tucson, Arizona, USA

*Correspondence
Ryota Fukai, Japan Aerospace Exploration Agency, 3-1-1 Yoshinodai, Chuo-ku, Sagamihara-shi, Kanagawa, Japan.
Email: fukai.ryohta@jaxa.jp

Abstract–Analyzing primitive extraterrestrial samples from asteroids is key to understanding the evolution of the early solar system. The OSIRIS-REx mission returned samples from the B-type asteroid Bennu, providing a valuable opportunity to compare them with the Ryugu samples collected by the Hayabusa2 mission. This study examines the representativeness of a fraction of the Bennu samples, which was allocated from NASA to JAXA, by nondestructive characterization of their physical and spectral properties without atmospheric exposure. The reflectance and observed spectral features in the visible-to-infrared range of the Bennu sample resemble those from the spectroscopic analysis of different fractions. Additionally, we found differences in the slope of the visible range and band-center of ~2.7 μm band between the samples and the asteroid surface, which could be explained by the degree of space weathering. A comparative analysis of the Bennu and Ryugu samples revealed spectral similarities, including absorption features indicative of Mg-rich phyllosilicates, organics, and carbonates, without any evidence of sampling bias or terrestrial alteration. This finding can be used as a benchmark for subsequent Ryugu–Bennu comparative studies.

INTRODUCTION

Research on the nature of multiple asteroids can strongly constrain the formation and evolution of stony and icy dust particles, pebbles, and planetesimals in the early solar system. The Origins, Spectral Interpretation, Resource Identification, Security-Regolith Explorer (OSIRIS-REx) mission of the National Aeronautics and Space Administration (NASA) launched a spacecraft on the B-type asteroid (101955) Bennu in 2016 and started a proximity operation in 2018. Samples were collected from the Bennu surface on October 20, 2020, and the sample

capsule was returned to Earth on September 24, 2023 (Lauretta et al., 2024). A fundamental aspect of the characterization of the asteroid Bennu involves a comparison with the data from the asteroid (162173) Ryugu, which was explored by the Hayabusa2 spacecraft (Tachibana et al., 2022; Yada et al., 2022). These asteroids exhibit fundamental similarities (Tatsumi et al., 2021), thereby providing crucial reference points for the early solar system.

The origin of the asteroids Bennu and Ryugu can be constrained by combining remote sensing data with the analyzed data of the returned samples from each asteroid object. The remotely sensed spectra of both Ryugu and Bennu exhibit a flat, dark profile with no noticeable absorption bands in the visible range (DellaGiustina et al., 2019; Sugita et al., 2019; Yumoto et al., 2024). These spectral characteristics, along with their cratering records and dynamic evolution simulations, suggest that these asteroids originate from a common collisional family—the Polana–Eulalia family (Bottke et al., 2015, 2020; de León et al., 2016; Walsh et al., 2024). This implies that the parent bodies of Ryugu and Bennu can be traced back to a common ancestral body. However, direct evidence from remote sensing observations confirming this hypothesis is lacking. For instance, the different types of exogenic boulders found on these asteroids indicate that their immediate parent bodies—the ones from which they directly accreted—were different (DellaGiustina et al., 2021; Tatsumi et al., 2021); however, this does not necessarily indicate that their earlier generation parent bodies were also different. The origin of the asteroid Ryugu was assessed by analyzing its bulk isotopic and elemental compositions (Nakamura et al., 2023; Okazaki et al., 2023; Yokoyama et al., 2023) as well as its mineralogy and texture (Loizeau et al., 2023; Nakamura et al., 2023; Pilorget et al., 2022, 2024). The O and nucleosynthetic Ti–Cr isotopic systems have indicated that Ryugu has originated from the outer solar system (Nakamura et al., 2022; Okazaki et al., 2023; Yokoyama et al., 2023). The presence of CO_2 fluid inclusions (Nakamura et al., 2023) and ammonium-rich salts (Pilorget et al., 2024) in the Ryugu samples also supports the formation of the parent body in the outer solar system. Comparative analyses of samples from Ryugu and Bennu are required to clarify whether the two asteroids originated from a common collisional family sharing a single parent body.

To facilitate a comparative analysis of the Ryugu and Bennu samples, the samples need to be maintained in a pristine environment to prevent any contamination by Earth's atmosphere during sample processing. For instance, immediate alteration of the sample by the terrestrial atmosphere and adsorption of terrestrial water have been reported in the Ryugu sample analysis (Imae et al., 2024;

Nakamura et al., 2023). Consequently, characterization of the Bennu sample without atmospheric exposure is critical for comparative studies of the Ryugu and Bennu samples. Constraints on the features of the Bennu sample can be obtained through sample characterization. First, especially in the case of samples shared between multiple curation facilities, the representativeness of the samples must be assessed to interpret their nature. Bulk sample description is performed using an optical microscope and spectroscopy at the visible and infrared wavelengths. This process is used to verify the representativeness of the samples (Fukai et al., 2024; Hatakeda et al., 2023; Yada et al., 2022). In addition, this information establishes a seamless connection between remote sensing and sample analysis. The spectral variation at the surface of the asteroid Bennu has been observed across the visible range (DellaGiustina et al., 2020), near-infrared (NIR) range (Clark et al., 2023), and thermal infrared range (Hamilton et al., 2021). Overall, it is essential to consider the relationship between bulk-scale samples and the asteroid surface when assessing the nature of the samples in question. Second, the variation observed within the Bennu samples should provide valuable insights for interpreting the intrinsic nature of the samples. Finally, a spectroscopic comparison with the Ryugu samples is valuable for assessing the origin and evolution of these asteroids.

In this study, we provide a preliminary description of the portion of the Bennu samples curated by the Japan Aerospace Exploration Agency (JAXA) using data from a series of microscopic nondestructive analyses, including Fourier Transform Infrared Spectroscopy (FT-IR), conducted within clean chambers without risking atmospheric exposure. These data were used to assess the representativeness and variability of the Bennu samples transferred from NASA to JAXA by comparing the data obtained from the Bennu samples in the JAXA curation facility with published data (Connolly and Lauretta et al., 2025; Lauretta and Connolly et al., 2024).

METHODS

Samples

A total of 0.5 wt% (Table 1) of the bulk Touch-and-Go Sample Acquisition Mechanism (TAGSAM) Bennu samples (121.6 g) was allocated to JAXA in accordance with the Memorandum of Understanding (MOU) between JAXA and NASA. The sample selection process for the bulk samples is described in the Supporting Information. The JAXA fraction was derived from OREX-800058-0, OREX-800111-0, OREX-800116-0, OREX-800120-0, and OREX-800125-0. The JAXA curation team renamed the fraction of OREX-800058-0 to ORX-19000, OREX-800111-0 to ORX-29000, OREX-800116-0 to

TABLE 1. Data from the five bulk samples.

	ORX-19000	ORX-29000	ORX-39000	ORX-49000	ORX-59000	Total
Sample weight (mg)[1]	182.43 ± 0.03	134.89 ± 0.04	152.40 ± 0.04	47.07 ± 0.03	147.60 ± 0.04	664.39 ± 0.08
CSFD[2] index	2.36 ± 0.08	2.55 ± 0.12	2.21 ± 0.10	3.18 ± 0.15	1.71 ± 0.07	2.29 ± 0.05
Reflectance (0.550 μm)	0.0219	0.0232	0.0242	0.0230	0.0237	0.0231 ± 0.0008
2.7-μm band center position (μm)[3]	2.714	2.713	2.713	2.713	2.713	2.713 ± 0.001
2.7-μm absorption depth (%)[4]	15.0	15.4	13.4	14.6	13.6	14.4 ± 0.9

[1]The errors represent the standard error (1SE) from the five replicate measurements.

[2]Cumulative size–frequency distribution.

[3]The error due to the resolution of wave number is ±0.0007 μm.

[4]The difference between the maximum and minimum reflectance value between 2.0 and 3.0 μm, normalized by the maximum reflectance in the same range.

ORX-39000, OREX-800120-0 to ORX-49000, and OREX-800125-0 to ORX-59000 on the Bennu sample database (https://darts.isas.jaxa.jp/app/curation/bennu/) published by JAXA.

Facility

The clean chamber (CC) for the Bennu samples was installed in an International Organization for Standardization (ISO) class 6 clean room within the curation facility at the Institute of Space and Astronautical Science (ISAS), JAXA. The CCs dedicated to the Bennu samples are CC5-1 and CC5-2; they are mainly made of electropolished 304 stainless steel and continuously purged with purified nitrogen gas. A companion paper describes the curation facility for the OSIRIS-REx samples, including the clean room and CCs (Tahara et al., 2025).

Instruments

An optical digital microscope (Keyence VHX-8000) has been positioned above the CC5-2 window to capture optical sample images. We obtained mapping data with the depth compositions of five bulk dish samples at a magnification of 100×. The CC5-2 is equipped with a microbalance A&D AD-4212D that can weigh 1 μg in a minimal digit display to measure weights of bulk and individual samples with a customized outer cover and a windshield of 6061 aluminum alloy. The net sample weight is obtained by subtracting the tare dish weight from the gross weight (see Tahara et al., 2025). The sample weight is determined as the mean of five repeated analyses. The sample weight error corresponds to the standard error (1SE). A μ-FT-IR JASCO IRT-5200/VIR-200 microscope has been installed over a chamber attached to CC5-2 to obtain NIR to mid-infrared (MIR) spectra (2.0 to ~13.0 μm in wavelength) through a BaF_2 viewport. The spectral resolution is 4 cm^{-1}, and the number of scans is 100. The background reflectance spectrum was obtained using a gold mirror that is not adapted to quantitatively determine the absolute reflectance value. The reflectance spectra of each bulk dish sample were obtained by averaging the mapping data consisting of 65–74 fields of view, each acquired with a 500-μm square aperture, except for the area where the surface of the sapphire dish was largely exposed (Figure S1). In addition, we remeasured the reflectance of relatively large particles in the point-by-point mode, and these measurements were also included in the averaging, as the mapping data for these grains were generally unfocused in the overall mapping mode. A multiband spectral microscope can also be installed above the CC5-2. This microscope, equipped with a monochrome CMOS camera and six-band filters at 0.39, 0.48, 0.55, 0.59, 0.70, and 0.85 μm, is identical to that used for the initial descriptions of the Ryugu samples (Cho et al., 2022). This set of wavelengths is compatible with the Optical Navigation Camera (ONC) filters onboard Hayabusa2. The incidence, emission, and phase angles of the multiband microscope were set as 30°, 0°, and 30°, respectively. The camera's field of view (FOV) was 5.6 mm × 2.9 mm, with an effective spatial resolution of ~10 μm. For each dish, 12 FOVs were measured to cover the entire ~180 mm^2 area of the samples. The data from these measurements were averaged to produce a single representative spectrum for each dish. The MicrOmega chamber unit connected to CC5-1 is equipped also with a NIR hyperspectral microscope (MicrOmega) to conduct further sample characterization. The MicrOmega results are presented in a separate paper (Pilorget et al., 2025).

RESULTS

Sample Weight

The total weights for the five bulk dish samples are 664.39 ± 0.08 mg. The weights for the individual dish
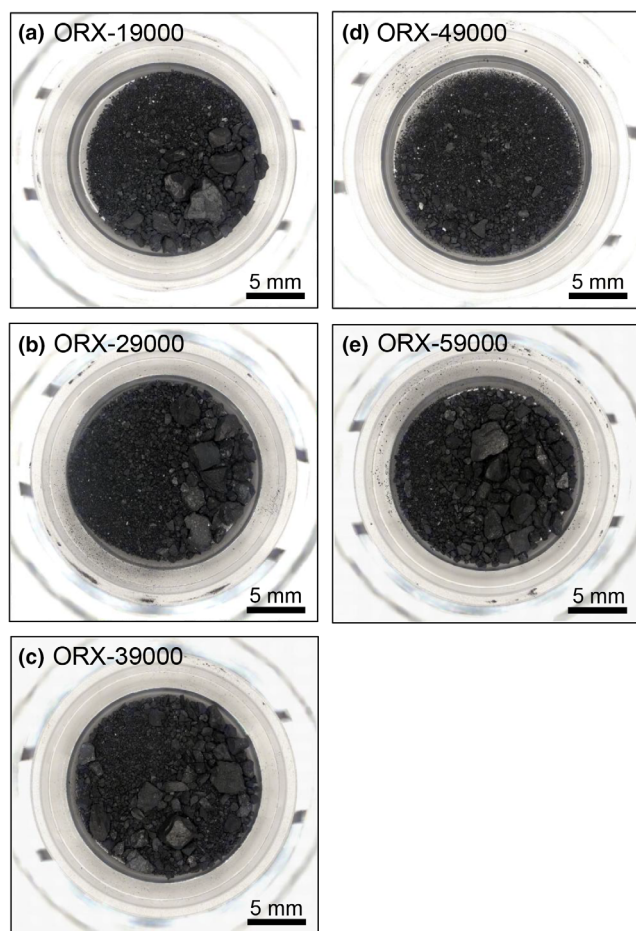
FIGURE 1. Photographs of the (a) ORX-19000, (b) ORX-29000, (c) ORX-39000, (d) ORX-49000, and (e) ORX-59000 samples.
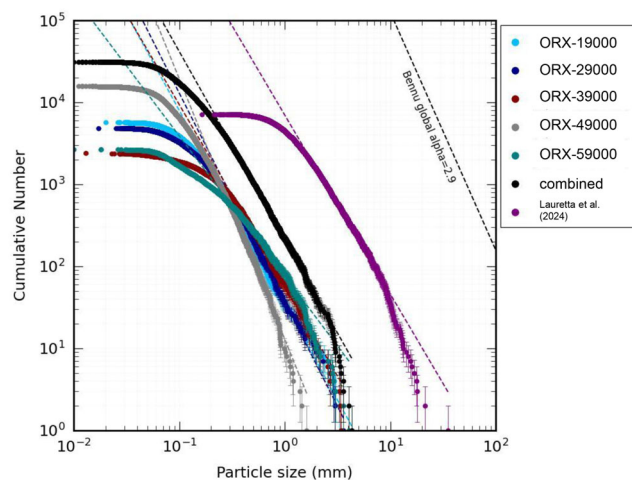

FIGURE 2. Particle size–frequency distribution of Bennu grains in the ORX-19000, ORX-29000, ORX-39000, ORX-49000, and ORX-59000 samples. The particle size–frequency distribution is derived from DellaGiustina et al. (2019).

samples obtained are 182.43 ± 0.03 mg (ORX-19000), 134.89 ± 0.04 mg (ORX-29000), 152.40 ± 0.04 mg (ORX-39000), 47.07 ± 0.03 mg (ORX-49000), and 147.60 ± 0.04 mg (ORX-59000). Errors indicate standard errors from replicate measurements (Tahara et al., 2025).

Optical Microscope Observation

Particles in the five bulk dishes (Figures 1 and S2–S5) show a variety of morphological characteristics, including angular, hummocky, and mottled grains, as reported by Lauretta et al. (2024) for the bulk samples. As consistent with Connolly et al. (2025), signatures of chondrules (ellipse-shaped inclusions; e.g., Simon et al., 2018) and refractory materials (typically fractured outline and white to brown color; e.g., Fukai et al., 2025; Tait et al., 2016), which usually exist within carbonaceous chondrites except for CI, were not identified in the bulk Bennu samples through the visual inspection of microscope images (Figures S2–S5).

We identified at least 30,000 Bennu particles from the microscopic images of five bulk sample dishes using a machine learning method (Shimizu et al., 2025). Figure 2 shows the relationship between the cumulative number of particles and the maximum Feret diameter of the particles in the individual bulk dishes. The power-law index values in the size–frequency distribution of the individual bulk dish samples were obtained by fitting for specific size ranges (Table 1). The power-law index values of the bulk dish samples range from −1.71 ± 0.07 (i.e., ORX-59000; particle size: 0.32 to 4.10 mm) to −3.18 ± 0.15 (i.e., ORX-49000; particle size: 0.32 mm to 1.60 mm).

Reflectance Spectroscopy

We obtained the reflectance spectra of five bulk samples in the visible-to-infrared wavelength range (Figures 3 and 4). The average reflectance of five bulk samples at 0.55 μm is 0.0231 ± 0.0008 (Table 1), with the range representing the standard deviation across the five bulk samples (Figure 3a). After normalizing the spectra at 0.55 μm, the average spectral slope within the 0.48–0.85 μm range is 0.22 ± 0.04 μm^{-1} (Figure 3b). The NIR spectrum of the five bulk samples shows absorption bands at ~2.7 μm attributed to OH stretching, at ~3.4 μm attributed to CH aliphatic stretching, and at ~3.4 and 3.95 μm indicating the presence of carbonate minerals (Figure 4a; Amano et al., 2023; Yada et al., 2022). The relative band depth of the ~2.7 μm feature in the average spectra for each dish ranges from 13.4% to 15.4% (Table 1). The average band center of the ~2.7 μm band for the five bulk dishes is 2.713 ± 0.001 μm (standard
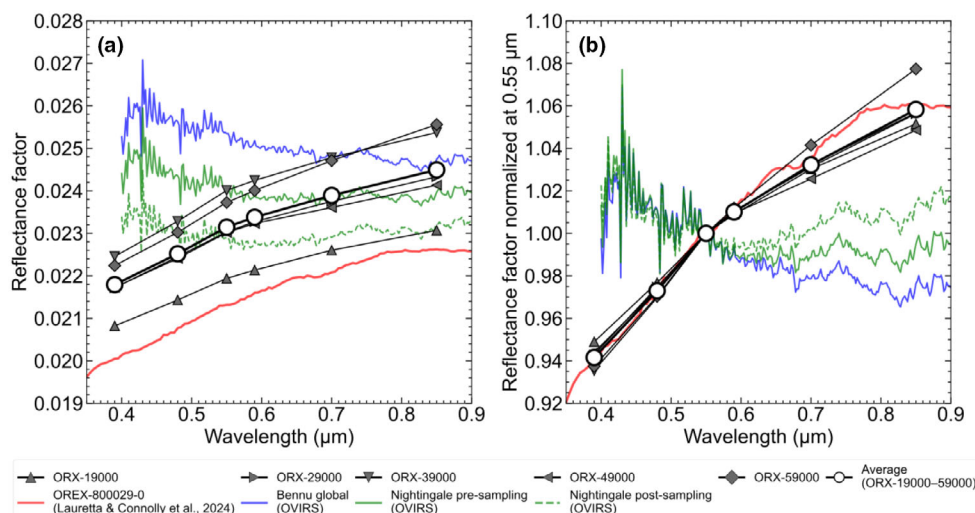
FIGURE 3. Reflectance spectra of the Bennu bulk samples in the visible range (a) before and (b) after normalization at 0.55 μm. The spectra are compared with measurements from the Reflectance Experiment Laboratory (RELAB; Lauretta et al., 2024) and remote sensing observations by OSIRIS-REx Visible and Infrared Spectrometer (OVIRS; Lauretta et al., 2024). The spectrum of a Bennu aggregate sample (OREX-800029-0) was measured at RELAB under the same photometric angles used in this study: (incidence angle, emission angle, phase angle) = (30°, 0°, 30°). The OVIRS spectra were photometrically corrected to the same (30°, 0°, 30°) condition.

deviation; Table 1), which indicates the presence of Mg-rich phyllosilicates (Beck et al., 2010; Takir et al., 2013). In the MIR wavelength range, we observed the absorption features around ~6.0 μm by C=C and/or CO_3^{2-} and/or H_2O (Figure 4b; Amano et al., 2023; Bishop et al., 2021; Kebukawa et al., 2020). Also, the Christiansen feature (CF) and the main Reststrahlen band (RB) of five bulk sample spectra appear at ~9.1 and ~9.8 μm, respectively, which indicates the presence of phyllosilicates (Figure 4c; e.g., saponite; Salisbury et al., 1987). Finally, the infrared reflectance spectra of several large grains in the ORX-19000, ORX-29000, ORX-39000, and ORX-59000 samples (spots on the right panels of Figure S1) show a variation for the peak positions and shapes of the ~2.7 μm band (~2.70–2.73 μm; Figure S6). The spectral variety of grains in the bulk dishes is also detailed in a separate paper focused on the MicrOmega results (Pilorget et al., 2025).

DISCUSSION

Representativeness of the Bennu Samples

Optical Microscope Observation

The microscopic images of the Bennu bulk samples (Figure 1) show similarities to the Advanced Imaging and Visualization of Astromaterials (AIVA) data of the Bennu samples in TAGSAM during the OSIRIS-REx curation phase. The ORX-19000 to ORX-59000 samples include three main types of morphologies (angular, hummocky,

and mottled grains; Figure S1), as defined by the OSIRIS-REx science team (Lauretta et al., 2024). In addition, no apparent signatures of chondrules or refractory materials are evident within the samples, which are consistent with the results of previous studies (Connolly et al., 2025; Lauretta et al., 2024). Collectively, these morphological features indicate that no significant sample bias exists between the NASA and JAXA collections.

High-resolution mapping data of the Bennu bulk dish samples acquired using the digital microscope are valuable for obtaining the particle size–frequency distribution. Particles from all the bulk dish samples show a distribution in which the power-law index ranges from −3.18 ± 0.15 (ORX-49000) to −1.71 ± 0.07 (ORX-59000), and the data combined with all the detected grains show −2.29 ± 0.05 (Figure 2; Table 1). This averaged value overlaps within error with the size–frequency distribution based on the longest axis of particles obtained from the AIVA data reported by a previous study (−2.18 ± 0.06; Lauretta et al., 2024). This suggests that the five bulk dish samples primarily represent the full size distribution, although the size scale used for the fitting differs between this study (~0.3 to ~4.0 mm) and the aforementioned previous study (~2.0 to ~10.0 mm; Lauretta et al., 2024). Notably, the power-law indices reported in this study and Lauretta et al. (2024) are both lower than those of the global boulders on Bennu (DellaGiustina et al., 2019), suggesting that a higher proportion of coarse particles is present in the returned samples.
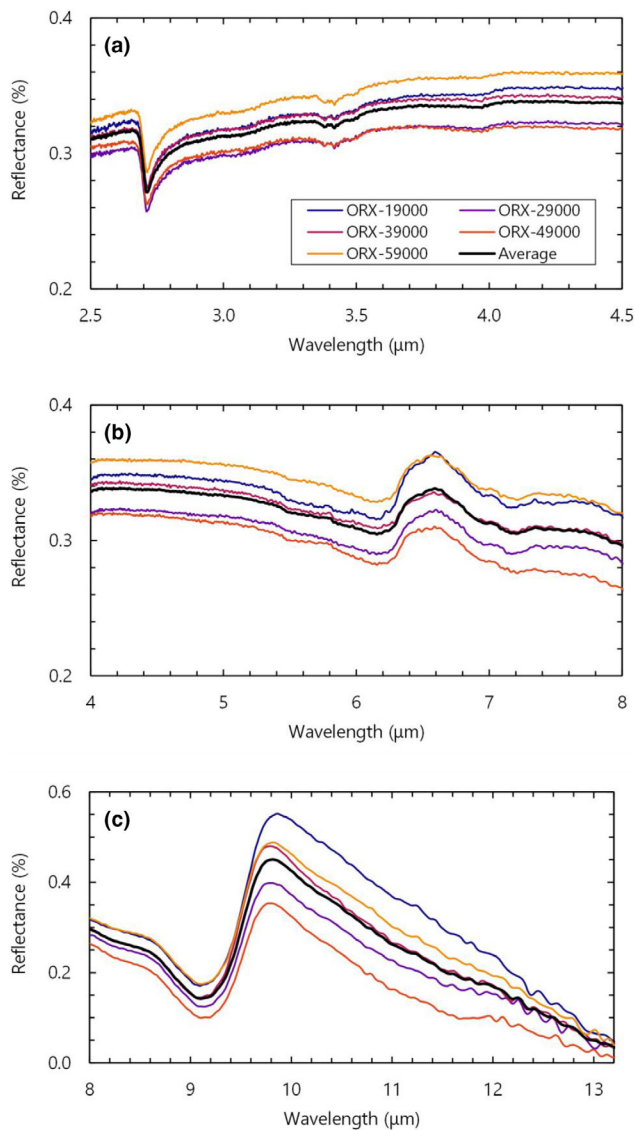
FIGURE 4. Near- and mid-infrared reflectance spectra of the Bennu bulk samples and their averages at (a) 2.5–4.5, (b) 4.0–8.0, and (c) 8.0–13.2 μm. Reflectance spectra were obtained with a gold mirror background.
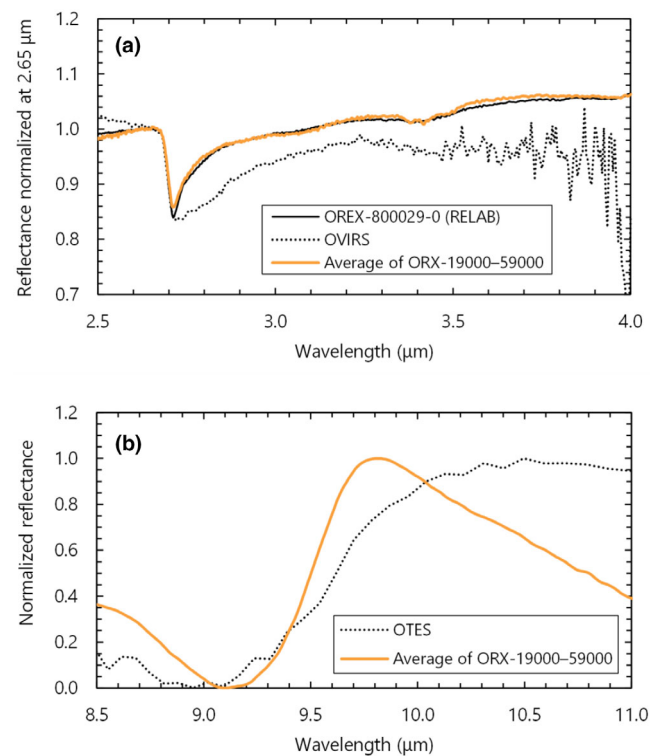

FIGURE 5. Near- and mid-infrared reflectance spectra averaged over the five Bennu bulk samples compared with remote sensing data. (a) Near-infrared reflectance spectrum within the 2–4-μm range of averaged ORX-19000 to ORX-59000 (orange line), OREX80029-0 sample acquired at the NASA Reflectance Experiment Laboratory (RELAB) (black line; Lauretta et al., 2024), and global spectrum of the asteroid Bennu (dotted line; Simon et al., 2021). The spectra are normalized by reflectance at 2.65 μm. The near-infrared reflectance spectrum of ORX-19000 to ORX-59000 was obtained with a gold mirror background. (b) Mid-infrared reflectance spectrum within the 8.5–11.0-μm range of averaged five Bennu bulk dish samples (orange line) and the global spectrum of the asteroid Bennu (dotted line; Hamilton et al., 2019), normalized as the minimum peak of Christiansen feature = 0 and maximum peak of Reststrahlen band = 1. The mid-infrared reflectance spectrum of ORX-19000 to ORX-59000 is obtained with a gold mirror background.

Spectral Comparison Between Collected Samples and the In-space Surface of Bennu

NIR–MIR

To assess the bulk-scale sample homogeneity, we compared the reflectance spectra of JAXA's fractions (ORX-19000 to ORX-59000) with those of NASA's fractions (OREX800029-0) measured at the NASA Reflectance Experiment Laboratory (RELAB) at Brown University (Lauretta et al., 2024). In the NIR range, the peak position, band depth, and spectral shape of the ~2.7-μm feature of the averaged JAXA's fraction are consistent with those of the OREX800029-0 sample (Figure 5). These spectral similarities between these samples at ~2.7 μm also support that the ORX-19000 to ORX-59000 samples were not altered (i.e., no water adsorption) during the sample transportation and initial curation phase at the Extraterrestrial Sample Curation Center (ESCuC). Also, the ~3.4 and 3.95 μm bands are observed both in the ORX-19000 to ORX-59000 and OREX800029-0 samples. Overall, the ORX-19000 to ORX-59000 and OREX800029-0 samples consist of similar types of components, as reflected by the bulk-scale NIR spectroscopy.

We also compared the reflectance spectra of the ORX-19000 to ORX-59000 samples with remote sensing observations using the OSIRIS-REx Visible and Infrared Spectrometer (OVIRS) to assess the representativeness of the collected samples at the asteroid scale. Figure 5 shows the infrared spectra of the Bennu samples obtained using FT-IR compared with the hyperspectral reflectance data obtained using OVIRS. Data from the Bennu bulk samples show a ~ 2.7-μm OH band centered at 2.72 μm with an asymmetric spectral shape (Figure 4a). In contrast, there is a 20-nm difference in the band center (2.74 ± 0.01 μm; Hamilton et al., 2019), and the OVIRS data exhibit a broader absorption band. The difference in the ~2.7-μm band center and the spectral shape is possibly due to the degree of surface weathering between the samples and the asteroid.

Thermal infrared spectral data from the OSIRIS-REx Thermal Emission Spectrometer (OTES) suggest that the peak position of CF on the global Bennu surface indicates the presence of phyllosilicate, which is most similar to CM chondrites (Hamilton et al., 2019). The ORX-19000 to ORX-59000 samples show a maximum peak position of CF that is consistent with that of the OTES data (Figure 5b). Conversely, the maximum peak of the RB of the averaged five bulk dishes is shifted toward a shorter wavelength compared with that of the OTES data by ~0.7 μm (Figure 5b; Hamilton et al., 2019). This shift seems consistent with the interpretation that the shift of the ~2.7-μm band could be due to surface weathering, as the weathered materials tend to show a peak at a higher wavelength (Lantz et al., 2024). In addition, the peaks in the MIR spectra are sensitive to environmental conditions controlled by physical parameters (e.g., Donaldson Hanna et al., 2012). Previous studies suggested that the particle size and fluctuation of the surface temperature at ~250 to ~400 K on the Bennu surface (Rozitis et al., 2020) only affect the peak position of RB by ≲0.1 μm (Amano et al., 2023; Poggiali et al., 2021). Instead, the peak shift in RB of the five bulk samples could be due to differences in the environmental conditions, including differences in pure nitrogen and vacuum (Bates et al., 2021; Donaldson Hanna et al., 2012).

Visible spectra

The visible spectra of the ORX-19000 to ORX-59000 samples are ~10% brighter than that of the OREX800029-0 sample reported in a previous study (Figure 3a; Lauretta et al., 2024). The difference in reflectance between the spectra of the Bennu samples measured in this study and that of the OREX800029-0 sample measured at RELAB does not necessarily invalidate the representativeness of the ORX-19000 to ORX-59000 samples. We consider the average reflectance

of each bulk dish sample to be strongly influenced by the abundance and orientations of large millimeter-sized particles, as significant reflectance variation was observed among different bulk dishes (2.19–2.42%; Table 1) and digital microscope images (Figure 1). For example, the surface areas of the facets oriented in specular configurations and the shadows cast by these grains play significant roles in determining the average reflectance of each sample dish. In contrast, the spectral shapes of the Bennu samples measured in this study, which are not strongly affected by large millimeter-sized grains, are remarkably consistent with those of the OREX800029-0 sampled at RELAB (Figure 3b), with a deviation of less than 0.5%.

All Bennu sample spectra examined in this study consistently exhibit positive spectral slopes as opposed to the negative spectral slope observed through remote sensing (Figure 3; Lauretta et al., 2024) and ground-based observations (Clark et al., 2011). Compared with the global average spectrum of Bennu, the Nightingale sampling site exhibits darker and redder spectra (Figure 3), which are assumed to represent materials least affected by space weathering (DellaGiustina et al., 2020). Furthermore, the gas released during the sampling process exposed the subsurface materials that are darker and redder than those observed before the sampling (Lauretta et al., 2022). The spectra of samples are even redder than the post-sampling observations of the sampling site across the entire 0.40–0.85-μm range (Figure 3b). The reflectance of the averaged five bulk sample spectra at 0.550 μm most closely aligns with that of the sampling site observed after sampling (Figure 3a). However, the pre-sampling reflectance remains within the range of variation observed across the five bulk samples (Figure 3a). This spectral discrepancy between the data in this study and the remote sensing data may be due to space weathering effects (e.g., Lantz et al., 2017; Matsuoka et al., 2023) and/or differences in physical properties (e.g., grain size and porosity) between the loosely packed materials on the asteroid surface and the subsurface from which the samples were collected (Walsh et al., 2022).

Spectroscopic Variation in the Bennu Samples

Bennu samples have been shown to preserve processes that may have occurred within the parent body and asteroid surface (Connolly et al., 2025; Keller et al., 2025; Lauretta et al., 2024; Zega et al., 2025). In the curation phase, a preliminary characterization is performed to determine the fundamental characteristics of the Bennu samples, excluding terrestrial contamination and sampling bias. The primary focus of this section is the spectroscopic

variation, through which potential trends associated with the physicochemical processes that occur on the parent body and asteroid can be documented.

Generally, the ORX-19000 to ORX-59000 samples show similar trends in spectral slope, absorption band position, and peak depth (Figures 3 and 4). In contrast, the power-law indices in the particle size–frequency distribution vary among the bulk samples, as seen in the slopes in Figure 2. The ORX-49000 sample contains the finest particles (Figure 2) and exhibits the lowest reflectance of RB intensity among those of the five bulk samples (Figure 4c), in accordance with the positive correlation between the reflectance of RB intensity and particle size (e.g., Pisello et al., 2023). However, the reflectance spectra of the bulk samples are also likely affected by the coarser particles within the dishes. For instance, the ORX-19000 sample exhibits a shift of the RB band to a longer wavelength compared with those of the other bulk samples (Figure 4c), which may be because it contains the largest particle within our collection.

We observed variation in the center positions of the ~2.7-μm band (~2.70–2.73 μm) within the ORX-19000–ORX-59000 area (Figure S6). One possible cause of the variation in the ~2.7-μm band is the change in the -OH structure of phyllosilicates due to space weathering (e.g., Lantz et al., 2017). Space weathering effects induce Fe enrichment within phyllosilicates; thus, the band center of weathered samples at ~2.7 μm tends to shift to longer wavelengths, resulting in a broader shape (Lantz et al., 2017). Broad shapes in the ~2.7-μm absorption band were obtained through the OVIRS data (Hamilton et al., 2019), supporting the hypothesis that most surface grains exhibit broad spectral shapes caused by space weathering. The Ryugu samples also experienced space weathering, showing a shift in the peak of the ~2.7-μm band toward longer wavelengths (Hiroi et al., 2023; Le Pivert-Jolivet et al., 2023). Additionally, aqueous alteration explains the spectral variation of the 2.7-μm band within phyllosilicates (Beck et al., 2010; Takir et al., 2019). Heavily aqueously altered (i.e., Mg-rich) phyllosilicates tend to show sharp band shapes and shorter peak positions on the ~2.7-μm band (e.g., Beck et al., 2010). Also, hydrated phosphorus-rich inclusions are observed within the Bennu samples (Pilorget et al., 2025), which can broaden the -OH peak (Pilorget et al., 2024).

The integration of this data set with a wide range of optical and spectroscopic data is crucial for elucidating the relationship between the spectral changes within phyllosilicates during planetesimal evolution and surface processes. First, the CF and RB positions can be shifted to shorter wavelengths because of the high degree of aqueous alteration that is similarly observed in carbonaceous chondrites (Beck et al., 2014). Furthermore, solar wind

implantation has been demonstrated to induce a prolonged peak shift in CF and RB, along with a 2.7-μm band peak shift (Lantz et al., 2017, 2024). Second, previous studies have suggested that redder near-ultraviolet slopes in asteroids are indicative of a lower degree of space weathering (Hendrix & Vilas, 2019) or a higher degree of aqueous alteration on the parent body (Tatsumi et al., 2023). Finally, the relationship between morphology and spectral variation can be discussed based on the characterization of individual particles, as demonstrated by the Ryugu samples (e.g., Nakato et al., 2023). However, the precision of reflectance spectra obtained with the multiband microscope and FT-IR at the bulk scale was found to be insufficient to assess their correlation with the ~2.7-μm band of Bennu particles. Also, the morphology of particles could not be determined accurately at the bulk scale. Subsequent to the bulk samples analyses, similar analyses on individual Bennu particles are ongoing by JAXA curation. These data sets obtained during the subsequent curation phase may shed light on the potential relationships among the morphology and visible, NIR, and MIR reflectance of the Bennu samples.

Comparison with the Ryugu Samples

A comparison of the reflectance spectrum data of the Bennu samples with those of Ryugu's characterization data, conducted nondestructively, is valuable because the Ryugu samples were obtained in a separate clean chamber with the same primary operation and maintenance system (e.g., Yada et al., 2022). The reflectance of the Bennu samples (Figure 6a) is consistent with the range of variation observed among the Ryugu samples (Matsuoka et al., 2023; Yada et al., 2022). Furthermore, the visible spectra of the ORX-19000 to ORX-59000 samples demonstrate positive spectral slopes without discernible absorption bands (Figure 6b), exhibiting a similarity to the Ryugu samples (Matsuoka et al., 2023; Yada et al., 2022). The slightly bluer spectral slope of the Ryugu samples may reflect their coarser grain size (Cantillo et al., 2023). The spectra of the Ryugu samples shown in Fig. 6 were measured on aggregates of millimeter-sized coarse grains (Matsuoka et al., 2023), whereas the Bennu samples analyzed in this study contain particles spanning a finer size range.

The analysis of the ORX-19000 to ORX-59000 samples and Ryugu bulk samples reveals a consistent presence of CI chondrite-related NIR spectra, characterized by the 2.7-μm absorption band, indicative of Mg-rich phyllosilicates, and the ~3.4- and 3.95-μm absorption bands, suggesting the presence of organics with aliphatic carbon and carbonates (Figure 7a; Pilorget et al., 2022; Yada et al., 2022). Notably, the Ryugu and Bennu samples exhibit significant similarities regarding
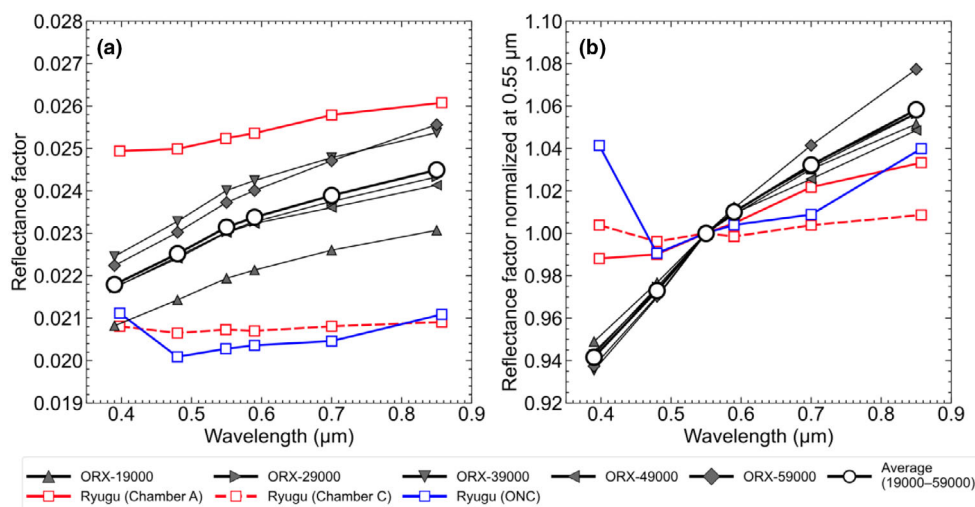
FIGURE 6. Reflectance spectra of the Bennu bulk samples compared with those of the Ryugu samples and asteroid Ryugu observed through remote sensing in the visible range (a) before and (b) after normalization at 0.550 μm. The spectra of Ryugu samples were measured on the surface of an aggregate composed of seven grains, each a few millimeters in size, collected from the first and second touchdowns (Chambers A and C), using an FT-IR spectrometer under the same photometric geometry as employed in this study (Matsuoka et al., 2023). The remote-sensing spectra of Ryugu observed by the Optical Navigation Camera were photometrically corrected to the same (30°, 0°, 30°) condition (Tatsumi et al., 2020).

the band centers and spectral shapes of the ~2.7-μm band; in contrast, they do not exhibit a distinct 3.0-μm peak that is frequently observed in CI chondrites (Takir et al., 2013). This finding indicates that the Ryugu and Bennu samples are devoid of adsorbed water within their matrices. The observed spectroscopic similarity of the Ryugu and Bennu samples regarding the ~2.7- and ~ 3.4-μm bands is consistent with the results obtained using MicrOmega (Pilorget et al., 2025).

Finally, we compare the MIR reflectance spectra of the ORX-19000 to ORX-59000 samples (Figure 7b,c) with those of the Ryugu coarse grains measured during the Hayabusa2 initial analysis phase (e.g., Nakamura et al., 2023). Within the MIR range, Ryugu and Bennu exhibit a similarity in the ~6-μm absorption due to the C=C and/or CO_3^{2-} and/or H_2O (Amano et al., 2023; Bishop et al., 2021; Kebukawa et al., 2020). In addition, the reflectance spectrum of the averaged ORX-19000 to ORX-59000 sample exhibits substantial CF and RB (Figure 7c). This finding suggests a potential similarity in the mineralogy of Ryugu and Bennu, with a prevalence of Mg-rich phyllosilicates, as evidenced in previous studies (Amano et al., 2023; Beck et al., 2014; Lauretta et al., 2024).

The spectroscopic similarity of Ryugu and Bennu, as observed at the bulk scale (sample weight >0.5 g) using FT-IR and MicrOmega, implies that these samples share similar intrinsic signatures and are free from sampling bias and the effects of terrestrial weathering. The intrinsic similarity of the Ryugu and Bennu samples is consistent for both the remote sensing and chemical analyses of the

samples (Bottke et al., 2015; Lauretta et al., 2024; Yokoyama et al., 2023). Furthermore, the Ryugu and Bennu samples exhibit CI-chondrite-related geochemical signatures, such as elemental abundance patterns and oxygen isotopic compositions (Lauretta et al., 2024; Yokoyama et al., 2023). Overall, the observed similarities between Ryugu and Bennu support a hypothesis of orbital evolution, with Ryugu and Bennu originating from the same asteroid family (Bottke et al., 2015; Campins et al., 2010).

The observed spectroscopic variations among the Bennu bulk samples discussed in the previous subsection and morphological variations among the distinct lithologies present within the Bennu samples (Connolly et al., 2025) constitute records of the thermal and mechanical evolution of the parent bodies of Bennu. It is hypothesized that Ryugu and Bennu may have undergone a distinct evolutionary trajectory, involving processes such as aqueous alteration, brecciation, and surface modification, within the asteroid population. A microscale study reveals that the Bennu samples exhibit a higher density of solar energy particle track ages (45,000 years) than that of the Ryugu samples (Keller et al., 2025). This finding indicates that the history of space weathering of the Bennu samples is more extensive than that of the Ryugu samples. Furthermore, the Bennu samples involve anhydrous minerals, such as olivine and pyroxene, at the micrometer scale (Lauretta et al., 2024; Pilorget et al., 2025). These minerals are present within a phyllosilicate matrix, which contrasts with the rarity of such mineral occurrences in the optical microscopic and
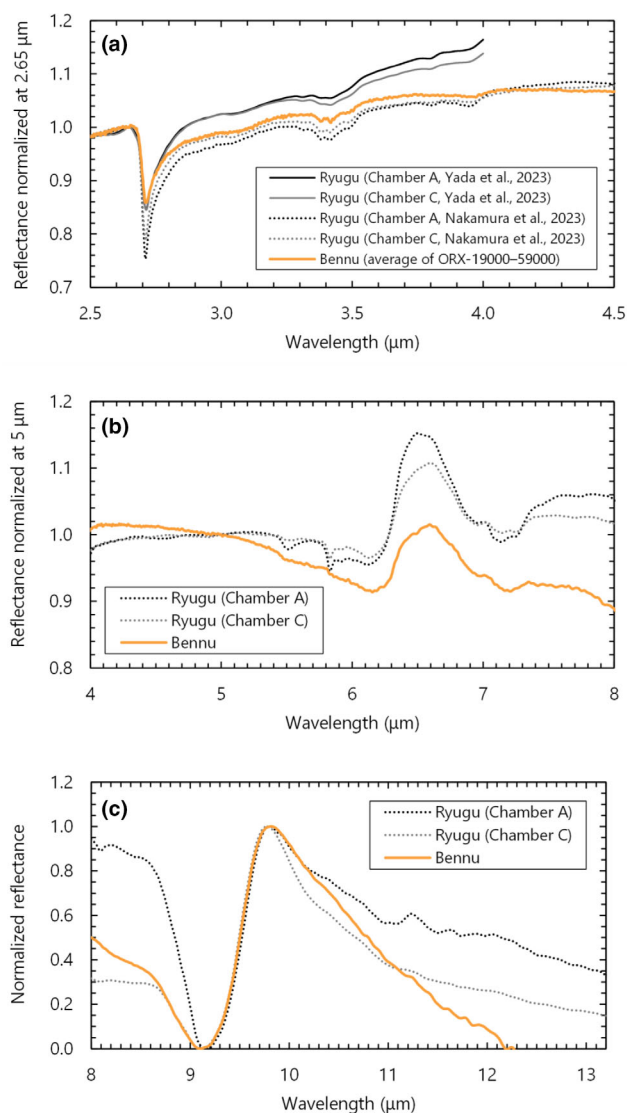
FIGURE 7. Near- and mid-infrared reflectance spectra of the averaged five Bennu bulk samples, obtained with a gold mirror background (orange line) compared with those of the Ryugu samples (black lines; Chambers A and C) (Yada et al., 2023 for panel (a); Nakamura et al., 2023 for panels (a)–(c)). (a) The spectra are normalized at 2.65 μm. (b) The spectra are normalized at 5 μm. (c) The spectra are normalized as the minimum peak of Christiansen feature = 0 and maximum peak of Reststrahlen band = 1.

infrared spectroscopic observations of the Ryugu samples (Pilorget et al., 2022, 2025). These potential differences in minerals between the Ryugu and Bennu samples can be attributed to the Bennu sample recording the aqueous alteration process with variable timing and location.

CONCLUSION

We nondestructively obtained bulk-scale data from the Bennu samples (i.e., ORX-19000 to ORX-59000)

and assessed their representativeness. The NIR spectra of the samples are similar to those obtained from a different sample fraction (Lauretta et al., 2024). This suggests that the ORX-19000 to ORX-59000 samples represent the general characteristics of the collected Bennu samples. In contrast, the slope observed in the visible range within ORX-19000–ORX-59000 is redder than that of the remote-sensing data. Also, there is a 20-nm difference in the band center of the ~2.7 μm band between ORX-19000–ORX-59000 and the remote sensing. The degree of space weathering may explain the differences observed between the samples and the asteroid.

We compared the visible and infrared reflectance spectra of the Bennu and Ryugu samples at the bulk scale. The peak position and spectral shape in the ~2.7-μm absorption band of the ORX-19000 and ORX-59000 samples are similar to those of the Ryugu samples. In addition, the spectral shape of the Bennu samples in the visible range matches well with that of the Ryugu sample. These observations suggest that the Ryugu and Bennu samples share a similar intrinsic signature (e.g., the presence of Mg-rich phyllosilicate and carbonate) without any sampling bias or terrestrial weathering effects, which could be a benchmark for subsequent Ryugu–Bennu comparative studies.

Characterization of the sample within the nitrogen glovebox, using optical microscopy and spectrometry, allowed the curation team to understand the nature of the sample, thereby eliminating concerns about volatile absorption. The homogeneity of this bulk sample and intrinsic spectral variation motivate curation activities, such as picking up particles from bulk samples and dividing them into aliquots. The scope of the sample analysis in various scientific fields can be derived from multiple curatorial data sets.

Data Availability Statement—The analysis data of ORX-19000, ORX-29000, ORX-39000, ORX-49000, and ORX-59000 is available via the "OSIRIS-REx Bennu Sample Curatorial Dataset" by the Astromaterials Science Research Group, Institut d'Astrophysique Spatiale, Université Paris-Saclay, CNES, S. Nakahara, K. Shimokoshi, K. Yumoto, S. Hayashi, S. Mori, Y. Aikyo,

Y. Cho, and S. Sugita (2025) (DOI: https://doi.org/10.17597/ISAS.DARTS/CUR-Bennu-description).

Editorial Handling—Dr. Daniel Glavin

REFERENCES

Amano, K., Matsuoka, M., Nakamura, T., Kagawa, E., Fujioka, Y., Potin, S. M., Hiroi, T., et al. 2023. Reassigning CI Chondrite Parent Bodies Based on Reflectance Spectroscopy of Samples from Carbonaceous Asteroid Ryugu and Meteorites. *Science Advances* 9: eadi3789.

Bates, H. C., Donaldson Hanna, K. L., King, A. J., Bowles, N. E., and Russell, S. S. 2021. A Spectral Investigation of Aqueously and Thermally Altered CM, CM-an, and CY Chondrites under Simulated Asteroid Conditions for Comparison with OSIRIS-REx and Hayabusa2 Observations. *Journal of Geophysical Research: Planets* 126: e2021JE006827.

Beck, P., Garenne, A., Quirico, E., Bonal, L., Montes-Hernandez, G., Moynier, F., and Schmitt, B. 2014. Transmission Infrared Spectra (2–25μm) of Carbonaceous Chondrites (CI, CM, CV–CK, CR, C2 Ungrouped): Mineralogy, Water, and Asteroidal Processes. *Icarus* 229: 263–277.

Beck, P., Quirico, E., Montes-Hernandez, G., Bonal, L., Bollard, J., Orthous-Daunay, F. R., Howard, K. T., et al. 2010. Hydrous Mineralogy of CM and CI Chondrites from Infrared Spectroscopy and their Relationship with Low Albedo Asteroids. *Geochimica et Cosmochimica Acta* 74: 4881–92.

Bishop, J. L., King, S. J., Lane, M. D., Brown, A. J., Lafuente, B., Hiroi, T., Roberts, R., Swayze, G. A., Lin, J. F., and Sanchez Roman, M. 2021. Spectral Properties of Anhydrous Carbonates and Nitrates. *Earth and Space Science* 8: e2021EA001844.

Bottke, W. F., Vokrouhlický, D., Ballouz, R. L., Barnouin, O. S., Connolly, H. C., Elder, C., Marchi, S., et al. 2020. Interpreting the Cratering Histories of Bennu, Ryugu, and Other Spacecraft-Explored Asteroids. *The Astronomical Journal* 160: 14.

Bottke, W. F., Vokrouhlický, D., Walsh, K. J., Delbo, M., Michel, P., Lauretta, D. S., Campins, H., Connolly, H. C., Scheeres, D. J., and Chelsey, S. R. 2015. In Search of the Source of Asteroid (101955) Bennu: Applications of the Stochastic YORP Model. *Icarus* 247: 191–217.

Campins, H., Morbidelli, A., Tsiganis, K., de León, J., Licandro, J., and Lauretta, D. 2010. The Origin of Asteroid 101955 (1999 Rq36). *The Astrophysical Journal* 721: L53–L57.

Cantillo, D. C., Reddy, V., Battle, A., Sharkey, B. N. L., Pearson, N. C., Campbell, T., Satpathy, A., De Florio, M., Furfaro, R., and Sanchez, J. 2023. Grain Size Effects on UV–MIR (0.2–14 μm) Spectra of Carbonaceous Chondrite Groups. *The Planetary Science Journal* 4: 177.

Cho, Y., Yumoto, K., Yabe, Y., Mori, S., Ogura, J. A., Yada, T., Miyazaki, A., et al. 2022. Development of a Multispectral Stereo-Camera System Comparable to Hayabusa2 Optical Navigation Camera (ONC-T) for Observing Samples Returned from Asteroid (162173) Ryugu. *Planetary and Space Science* 221: 105549.

Clark, B. E., Binzel, R. P., Howell, E. S., Cloutis, E. A., Ockert-Bell, M., Christensen, P., Barucci, M. A., et al. 2011. Asteroid (101955) 1999 RQ36: Spectroscopy from 0.4 to 2.4 μm and Meteorite Analogs. *Icarus* 216: 462–475.

Clark, B. E., Sen, A., Zou, X. D., DellaGiustina, D. N., Sugita, S., Sakatani, N., Thompson, M., et al. 2023. Overview of the Search for Signs of Space Weathering on the Low-Albedo Asteroid (101955) Bennu. *Icarus* 400: 115563.

Connolly, H. C., Lauretta, D. S., McCoy, T. J., Russell, S. S., Haenecour, P., Polit, A., Barnes, J. J., et al. 2025. An Overview of the Petrography and Petrology of Particles from Aggregate Sample from Asteroid Bennu. *Meteoritics & Planetary Science* 60: 979–996.

de León, J., Pinilla-Alonso, N., Delbo, M., Campins, H., Cabrera-Lavers, A., Tanga, P., Cellino, A., et al. 2016. Visible Spectroscopy of the Polana–Eulalia Family Complex: Spectral Homogeneity. *Icarus* 266: 57–75.

DellaGiustina, D. N., Burke, K. N., Walsh, K. J., Smith, P. H., Golish, D. R., Bierhaus, E. B., Ballouz, R. L., et al. 2020. Variations in Color and Reflectance on the Surface of Asteroid (101955) Bennu. *Science* 370: 6517.

DellaGiustina, D. N., Emery, J. P., Golish, D. R., Rozitis, B., Bennett, C. A., Burke, K. N., Ballouz, R. L., et al. 2019. Properties of Rubble-Pile Asteroid (101955) Bennu from OSIRIS-REx Imaging and Thermal Analysis. *Nature Astronomy* 3: 341–351.

DellaGiustina, D. N., Kaplan, H. H., Simon, A. A., Bottke, W. F., Avdellidou, C., Delbo, M., Ballouz, R. L., et al. 2021. Exogenic Basalt on Asteroid (101955) Bennu. *Nature Astronomy* 5: 31–38.

Donaldson Hanna, K. L., Wyatt, M. B., Thomas, I. R., Bowles, N. E., Greenhagen, B. T., Maturilli, A., Helbert, J., and Paige, D. A. 2012. Thermal Infrared Emissivity Measurements under a Simulated Lunar Environment: Application to the Diviner Lunar Radiometer Experiment. *Journal of Geophysical Research: Planets* 117: E00H05.

Fukai, R., Takeda, Y., Masuda, Y., Yamamoto, D., Iba, Y., Sasaki, S., Ikegami, S., Kubota, A., Sato, R., and Usui, T. 2025. The Bright-Field Grinding Tomography of Coarse-Grained Calcium-Aluminum-Rich Inclusions in the Allende Meteorite. *Icarus* 439: 116648.

Fukai, R., Usui, T., Fujiya, W., Takano, Y., Bajo, K. i., Beck, A., Bonato, E., et al. 2024. Curation Protocol of Phobos Sample Returned by Martian Moons eXploration. *Meteoritics & Planetary Science* 59: 321–337.

Hamilton, V. E., Christensen, P. R., Kaplan, H. H., Haberle, C. W., Rogers, A. D., Glotch, T. D., Breitenfeld, L. B., et al. 2021. Evidence for Limited Compositional and Particle Size Variation on Asteroid (101955) Bennu from Thermal Infrared Spectroscopy. *Astronomy & Astrophysics* 650: A120.

Hamilton, V. E., Simon, A. A., Christensen, P. R., Reuter, D. C., Clark, B. E., Barucci, M. A., Bowles, N. E., et al. 2019. Evidence for Widespread Hydrated Minerals on Asteroid (101955) Bennu. *Nature Astronomy* 3: 332–340.

Hatakeda, K., Yada, T., Abe, M., Okada, T., Nakato, A., Yogata, K., Miyazaki, A., et al. 2023. Homogeneity and Heterogeneity in Near-Infrared FTIR Spectra of Ryugu Returned Samples. *Earth, Planets and Space* 75: 46.

Hendrix, A. R., and Vilas, F. 2019. C-Complex Asteroids: UV-Visible Spectral Characteristics and Implications for Space Weathering Effects. *Geophysical Research Letters* 46: 14307–17.

Hiroi, T., Milliken, R. E., Robertson, K. M., Schultz, C. D., Amano, K., Nakamura, T., Yurimoto, H., et al. 2023. Evidence of Global Space Weathering by Solar Wind on Asteroid 162173 Ryugu. *Icarus* 406: 115755.

Imae, N., Tomioka, N., Uesugi, M., Kimura, M., Yamaguchi, A., Ito, M., Greenwood, R. C., et al. 2024. Mineralogical Approach on Laboratory Weathering of Uncontaminated Ryugu Particles: Comparison with Orgueil and Perspective for Storage and Analysis. *Meteoritics & Planetary Science* 59: 1705–22.

Kebukawa, Y., Nakashima, S., Mita, H., Muramatsu, Y., and Kobayashi, K. 2020. Molecular Evolution during Hydrothermal Reactions from Formaldehyde and Ammonia Simulating Aqueous Alteration in Meteorite Parent Bodies. *Icarus* 347: 113827.

Keller, L. P., Thompson, M. S., Seifert, L. B., Melendez, L. E., Thomas-Keprta, K. L., Le, L., Snead, C. J., et al. 2025. Space Weathering Effects in Bennu Asteroid Samples. *Nature Geoscience* 18: 825–831.

Lantz, C., Brunetto, R., Barucci, M. A., Fornasier, S., Baklouti, D., Bourçois, J., and Godard, M. 2017. Ion Irradiation of Carbonaceous Chondrites: A New View of Space Weathering on Primitive Asteroids. *Icarus* 285: 43–57.

Lantz, C., Nakamura, T., Baklouti, D., Brunetto, R., Henault, E., Kobayashi, S., Mivumbi, O., et al. 2024. Mid-Infrared Measurements of Ion-Irradiated Carbonaceous Meteorites: How to Better Detect Space Weathering Effects. *The Planetary Science Journal* 5: 201.

Lauretta, D. S., Adam, C. D., Allen, A. J., Ballouz, R. L., Barnouin, O. S., Becker, K. J., Becker, T., et al. 2022. Spacecraft Sample Collection and Subsurface Excavation of Asteroid (101955) Bennu. *Science* 377: 285–291.

Lauretta, D. S., Connolly, H. C., Aebersold, J. E., Alexander, C. M. O. D., Ballouz, R. L., Barnes, J. J., Bates, H. C., et al. 2024. Asteroid (101955) Bennu in the Laboratory: Properties of the Sample Collected by OSIRIS-REx. *Meteoritics & Planetary Science* 59: 2453–86.

Le Pivert-Jolivet, T., Brunetto, R., Pilorget, C., Bibring, J. P., Nakato, A., Hamm, V., Hatakeda, K., et al. 2023. Space Weathering Record and Pristine State of Ryugu Samples from Micromega Spectral Analysis. *Nature Astronomy* 7: 1445–53.

Loizeau, D., Pilorget, C., Riu, L., Brunetto, R., Bibring, J. P., Nakato, A., Aléon-Toppani, A., et al. 2023. Constraints on Solar System Early Evolution by Micromega Analysis of Ryugu Carbonates. *Nature Astronomy* 7: 391–97.

Matsuoka, M., Kagawa, E.-i., Amano, K., Nakamura, T., Tatsumi, E., Osawa, T., Hiroi, T., et al. 2023. Space Weathering Acts Strongly on the Uppermost Surface of Ryugu. *Communications Earth & Environment* 4: 1.

Nakamura, E., Kobayashi, K., Tanaka, R., Kunihiro, T., Kitagawa, H., Potiszil, C., Ota, T., et al. 2022. On the Origin and Evolution of the Asteroid Ryugu: A Comprehensive Geochemical Perspective. *Proceedings of the Japan Academy. Series B, Physical and Biological Sciences* 98: 227–282.

Nakamura, T., Matsumoto, M., Amano, K., Enokido, Y., Zolensky, M. E., Mikouchi, T., Genda, H., et al. 2023. Formation and Evolution of Carbonaceous Asteroid Ryugu: Direct Evidence from Returned Samples. *Science* 379: eabn8671.

Nakato, A., Yada, T., Nishimura, M., Yogata, K., Miyazaki, A., Nagashima, K., Hatakeda, K., et al. 2023. Variations of the Surface Characteristics of Ryugu Returned Samples. *Earth, Planets and Space* 75: 1.

Okazaki, R., Marty, B., Busemann, H., Hashizume, K., Gilmour, J. D., Meshik, A., Yada, T., et al. 2023. Noble Gases and Nitrogen in Samples of Asteroid Ryugu Record its Volatile Sources and Recent Surface Evolution. *Science* 379: eabo0431.

Pilorget, C., Baklouti, D., Bibring, J. P., Brunetto, R., Ito, M., Franchi, I., Tomioka, N., et al. 2024. Phosphorus-Rich Grains in Ryugu Samples with Major Biochemical Potential. *Nature Astronomy* 8: 1529–35.

Pilorget, C., Okada, T., Bibring, J. P., Loizeau, D., Hatakeda, K., Nardelli, L., Riu, L., et al. 2025. Bennu and Ryugu Constituents from Samples IR Analyses and Potential Source of Terrestrial Planets' Ingredients. *Nature Communications* 16: 9532.

Pilorget, C., Okada, T., Hamm, V., Brunetto, R., Yada, T., Loizeau, D., Riu, L., et al. 2022. First Compositional Analysis of Ryugu Samples by the Micromega Hyperspectral Microscope. *Nature Astronomy* 6: 221–25.

Pisello, A., Bisolfati, M., Poggiali, G., Tolomei, P., Braschi, E., Brucato, J. R., and Perugini, D. 2023. Mid-Infrared (MIR) Spectroscopy of Silicate Glasses as Analogs for Mercury's Surface: The Influence of Grain Size. *Minerals* 13: 170.

Poggiali, G., Brucato, J. R., Dotto, E., Ieva, S., Barucci, M. A., and Pajola, M. 2021. Temperature Dependent Mid-Infrared (5–25 mm) Reflectance Spectroscopy of Carbonaceous Meteorites and Minerals: Implication for Remote Sensing in Solar System Exploration. *Icarus* 354: 114040.

Rozitis, B., Emery, J. P., Siegler, M. A., Susorney, H. C. M., Molaro, J. L., Hergenrother, C. W., and Lauretta, D. S. 2020. Implications for Ice Stability and Particle Ejection from High-Resolution Temperature Modeling of Asteroid (101955) Bennu. *Journal of Geophysical Research: Planets* 125: e2019JE006323.

Salisbury, J. W., Hapke, B., and Eastes, J. W. 1987. Usefulness of Weak Bands in Midinfrared Remote Sensing of Particulate Planetary Surfaces. *Journal of Geophysical Research: Solid Earth* 92: 702–710.

Shimizu, Y., Miyamoto, H., and Michel, P. 2025. Diverse Evolutionary Pathways of Spheroidal Asteroids Driven by Rotation Rate. *Scientific Reports* 15: 10284.

Simon, A. A., Reuter, D. C., and Lauretta, D. S. 2021. Derivation of the Final OSIRIS-REx OVIRS in-Flight Radiometric Calibration. *Journal of Astronomical Telescopes, Instruments, and Systems* 7: 020501.

Simon, J. I., Cuzzi, J. N., McCain, K. A., Cato, M. J., Christoffersen, P. A., Fisher, K. R., Srinivasan, P., Tait, A. W., Olson, D. M., and Scargle, J. D. 2018. Particle Size Distributions in Chondritic Meteorites: Evidence for Pre-Planetesimal Histories. *Earth and Planetary Science Letters* 494: 69–82.

Sugita, S., Honda, R., Morota, T., Kameda, S., Sawada, H., Tatsumi, E., Yamada, M., et al. 2019. The Geomorphology, Color, and Thermal Properties of Ryugu: Implications for Parent-Body Processes. *Science* 364: 252.

Tachibana, S., Sawada, H., Okazaki, R., Takano, Y., Sakamoto, K., Miura, Y. N., Okamoto, C., et al. 2022. Pebbles and Sand on Asteroid (162173) Ryugu: In Situ Observation and Particles Returned to Earth. *Science* 375: 1011–16.

Tahara, R., Hatakeda, K., Nishimura, M., Yogata, K., Fukai, R., Miyazaki, A., Yada, T., et al. 2025. JAXA

Curation for Bennu Samples Returned by the NASA's OSIRIS-Rex Mission. *Meteoritics and Planetary Science* in press.

Tait, A. W., Fisher, K. R., Srinivasan, P., and Simon, J. I. 2016. Evidence for Impact Induced Pressure Gradients on the Allende CV3 Parent Body: Consequences for Fluid and Volatile Transport. *Earth and Planetary Science Letters* 454: 213–224.

Takir, D., Emery, J. P., McSween, H. Y., Hibbitts, C. A., Clark, R. N., Pearson, N., and Wang, A. 2013. Nature and Degree of Aqueous Alteration in CM and CI Carbonaceous Chondrites. *Meteoritics & Planetary Science* 48: 1618–37.

Takir, D., Stockstill-Cahill, K. R., Hibbitts, C. A., and Nakauchi, Y. 2019. 3-μm Reflectance Spectroscopy of Carbonaceous Chondrites under Asteroid-Like Conditions. *Icarus* 333: 243–251.

Tatsumi, E., Sakatani, N., Riu, L., Matsuoka, M., Honda, R., Morota, T., Kameda, S., et al. 2021. Spectrally Blue Hydrated Parent Body of Asteroid (162173) Ryugu. *Nature Communications* 12: 5837.

Tatsumi, E., Sugimoto, C., Riu, L., Sugita, S., Nakamura, T., Hiroi, T., Morota, T., et al. 2020. Collisional History of Ryugu's Parent Body from Bright Surface Boulders. *Nature Astronomy* 5: 39–45.

Tatsumi, E., Vilas, F., de León, J., Popescu, M., Hasegawa, S., Hiroi, T., Tinaut-Ruano, F., and Licandro, J. 2023. Near-Ultraviolet Absorption Distribution of Primitive Asteroids from Spectrophotometric Surveys. *Astronomy & Astrophysics* 672: A189.

Walsh, K. J., Ballouz, R. L., Bottke, W. F., Avdellidou, C., Connolly, H. C., Jr., Delbo, M., DellaGiustina, D. N., et al. 2024. Numerical Simulations Suggest Asteroids (101955) Bennu and (162173) Ryugu Are Likely Second or Later Generation Rubble Piles. *Nature Communications* 15: 5653.

Walsh, K. J., Ballouz, R. L., Jawin, E. R., Avdellidou, C., Barnouin, O. S., Bennett, C. A., Bierhaus, E. B., et al. 2022. Near-Zero Cohesion and Loose Packing of Bennu's near Subsurface Revealed by Spacecraft Contact. *Science Advances* 8: eabm6229.

Yada, T., Abe, M., Okada, T., Nakato, A., Yogata, K., Miyazaki, A., Hatakeda, K., et al. 2022. Preliminary Analysis of the Hayabusa2 Samples Returned from C-Type Asteroid Ryugu. *Nature Astronomy* 6: 214–220.

Yokoyama, T., Nagashima, K., Nakai, I., Young, E. D., Abe, Y., Aleon, J., Alexander, C. M. O., et al. 2023. Samples Returned from the Asteroid Ryugu are Similar to Ivuna-Type Carbonaceous Meteorites. *Science* 379: eabn7850.

Yumoto, K., Tatsumi, E., Kouyama, T., Golish, D. R., Cho, Y., Morota, T., Kameda, S., et al. 2024. Comparison of Optical Spectra between Asteroids Ryugu and Bennu: I. Cross Calibration between Hayabusa2/ONC-T and OSIRIS-Rex/Mapcam. *Icarus* 417: 116122.

Zega, T. J., McCoy, T. J., Russell, S. S., Keller, L. P., Gainsforth, Z., Singerling, S. A., Manga, V. R., et al. 2025. Mineralogical Evidence for Hydrothermal Alteration of Bennu Samples. *Nature Geoscience* 18: 832–39.

SUPPORTING INFORMATION

Additional supporting information may be found in the online version of this article.

Figure S1. Fourier Transform Infrared Spectroscopy analysis areas for mapping measurements of five bulk dishes.

Figure S2. Typical grains in the ORX-19000 sample.

Figure S3. Typical grains in the ORX-29000 sample.

Figure S4. Typical grains in the ORX-39000 sample.

Figure S5. Typical grains in the ORX-59000 sample.

Figure S6. Reflectance spectra of individual areas within the ORX-19000, ORX-29000, ORX-39000, and ORX-59000 samples.

Figure S7. (a) A color-enhanced image of OREX-800012, that is, tray A3. An area circled with a blue rectangle was requested from JAXA for the first sample separation in October 2023. (b) An image of OREX-800012 after the first separation for JAXA allocation. Three concavities in the aggregate samples, located near the upper left wall of the tray, are traces of the sample separations corresponding to the blue rectangle area in panel (a). The Advanced Imaging & Visualization of Astromaterials team took the original images at the NASA Johnson Space Center.

Figure S8. Optical images of (a) OREX-800001, (b) OREX-800005, (c) OREX-800007, and (d) OREX-800008, which were selected for the second sample separation for JAXA's allocation.

Figure S9. Color-enhanced images of (a) OREX-800001, (b) OREX-800005, (c) OREX-800007, and (d) OREX-800008, in which areas of sample separation request are indicated by yellow rectangles. Three enhanced colors of particles, namely red, green, and blue, are included in the areas.

Figure S10. Optical images of (a) OREX-800001, (b) OREX-800005, (c) OREX-800007, and (d) OREX-800008 after the sample separation by the NASA/Johnson Space Center curation team.

Figure S11. An optical microscopic image of contact pad #22 (OREX464000-0) allocated to JAXA. The diameter of the pad is ~3 cm.

Figure S12. Artifact spectrum found in blank measurement and its influence on the bulk sample (ORX-19000) spectrum. The artifact spectrum is an average of 500 spectra by spectral stacking.

Figure S13. Artifact spectra obtained on August 13–15, 18, 2025. Each spectrum is an average of 6000 spectra obtained by spectral stacking. The averaged spectrum was used for correction.

Figure S14. Bulk sample (ORX-19000) spectrum before and after correction. Absorption bands corresponding to the artifact spectrum were removed by the correction.

Figure S15. Reflectance spectra of the Bennu bulk samples and their average (a) before and (b) after the smoothing process, both normalized to 2.65–4.10 μm linear continuum.

Figure S16. Reflectance spectra of the Bennu bulk samples obtained with an InfraGold background. (a) Normalized at 2.65 μm, (b) normalized at 2.5 μm, and (c) normalized as the minimum peak of Christiansen feature = 0 and maximum peak of Reststrahlen band = 1.

Table S1. Instrument settings for Fourier Transform Infrared Spectroscopy mapping of bulk samples.